

Quantum phases in p -orbital degenerated attractive 1D fermionic optical lattices

Keita Kobayashi,¹ Yukihiro Ota,¹ Masahiko Okumura,¹ Susumu Yamada,^{1,2} and Masahiko Machida^{1,2}

¹CCSE, Japan Atomic Energy Agency, 5-1-5 Kashiwanoha, Kashiwa, Chiba 277-8587, Japan

²Computational Materials Science Research Team, RIKEN AICS, Kobe, Hyogo 650-0047, Japan

(Dated: June 24, 2021)

We examine quantum phases emerged by double degeneracy of p -orbital bands in attractive atomic Fermi gases loaded on a 1D optical lattice. Our numerical simulations by the density-matrix renormalization group predict the emergence of a state with a charge excitation gap, the Haldane insulator phase. A mapping onto an effective spin-1 model reveals its physical origin. Moreover, we show that population imbalance leads to richer diversity of the quantum phases, including a phase-separated polarized state. Finally, we study the effects of harmonic trap potential in this 1D chain.

PACS numbers: 67.85.Lm, 67.85.-d, 71.10.Fd, 75.40.Mg

I. INTRODUCTION

Optical lattice formed by interference of counter propagating laser beams is one of the most fruitful technical inventions in the progress of atomic gas physics [1]. The seminal reports (see, e.g., Ref. [2]) indicate that this system is regarded as a quantum simulator to emulate electronic structures in solid-state systems, with controllability of model parameters and flexibility of lattice geometric structures. The interaction is widely tuned from strongly-attractive to repulsive couplings by the Feshbach resonance. The different lattice structures, such as a 1D chain, bipartite square 2D lattice [3] like High- T_c cuprate superconductors, and frustrated triangular lattices [4] are available by tuning laser interference.

Simulating solid-state electronic structures in optical lattices requires treating the orbital degrees of freedom, as well as the charge and the spin degrees. Orbital degeneracy plays a crucial role in transition metals, for example. Such materials are currently targets in applied physics, owing to their wide usage of various industrial scene. Ultracold atomic gases with multiple band-degeneracy enable us to directly address quantum phenomena associated with the orbital degrees [3, 5–12]. In this paper, focusing on p -orbitals next higher to the lowest s -orbital, we show that the low-lying double degenerate orbitals lead to a rich phase structure of the ground states in an attractively interacting 1D chain (see Fig. 1). All the numerical calculations are done by the density matrix renormalization method (DMRG) (See, e.g., Refs. [13, 14]). We also derive an effective model to clarify the origin of the resultant quantum phase.

To identify the ground state in a many-body system is a primary issue for understanding quantum many-body effects. The nature of the ground state depends on the degeneracy intrinsic to a many-body system. In our system, the p -orbital degeneracy is a key ingredient of the various quantum phases. The p -orbitals in a 1D chain along z -axis lead to double degeneracy with respect to p_x and p_y orbitals, as seen in Fig. 1.

In this paper, we list up the ground-state properties in this attractive 1D chain. First, we show that the *inter-*

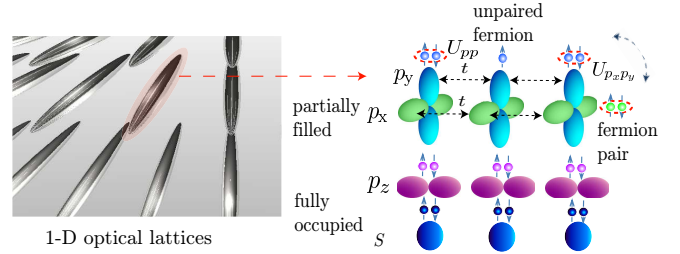


FIG. 1: (Color Online) Schematic diagram of fermionic gases on an optical lattice, with multiple bands (multi-band Hubbard chain). The intra-orbital interaction (U_{pp}) forms fermion pairs. The fermion pairs hop between different orbitals, by the pair-hopping interaction ($U_{p_x p_y}$) [see Eq. (3)].

orbital interaction leads to the emergence of the Haldane phase [18], close to half-filling. Below half-filling, the Luther-Emery phase [15] occurs, in the same way as *single-band* attractive Hubbard chains [16, 17]. In contrast to the gapless charge excitations in the Luther-Emery phase, the Haldane phase brings about a charge gapped feature. We remark that the Haldane phase with a charge excitation gap, a nonlocal string order, and edge states is known as a Haldane insulator phase [19–24]. This realization is proposed in bosonic chains with dipole interaction [19–22] and multi-component fermionic chains [23, 24]. A two-leg spin-1/2 ladder also shows the presence of a similar gapped phase [25]. Our numerical calculations and effective model reveal the occurrence of such an intriguing insulator phase in the present system. Next, in the presence of population imbalance, we show that a phase separation of polarized components occurs in a low fermion-pair-density case. This behavior comes from the double exchange interaction [26, 27] between Fermion pairs. Finally, we study an effect of trap potential. We propose that the trapped system allows the direct verification of the Haldane gap and the phase-separated polarized phase.

This paper is organized as follows. The p -orbitals 1D Hubbard Hamiltonian is derived in Sec. II. In Sec. IIIA, applying the DMRG method to this model, we calculate

the ground-state of the p -orbitals 1D chain, and we show the presence of the charge gap and the edge state. Furthermore, deriving an effective spin-1 Hamiltonian, the realization of the Haldane insulator phase is more evident. Section IIIB shows the results with population imbalance. We suggest a phase separation of polarized components. This phenomenon is explained, in terms of the double exchange interaction between fermion-pair particles. The effect of harmonic trap potential is shown in Sec. IIIC. Section IV is devoted to the summary.

II. MODEL

We start with the Hamiltonian for two-component Fermi gases,

$$H = \sum_{\sigma=\uparrow,\downarrow} \int d^3\mathbf{x} \left(\psi_{\sigma}^{\dagger} h \psi_{\sigma} + \frac{g}{2} \psi_{\sigma}^{\dagger} \psi_{\sigma}^{\dagger} \psi_{\sigma} \psi_{\sigma} \right), \quad (1)$$

with $h = -(\hbar^2/2m)\nabla^2 + V_{\text{opt}}(\mathbf{x})$ and two body interaction g . The optical lattice potential is $V_{\text{opt}}(\mathbf{x}) = \sum_{\alpha=x,y,z} V_{\alpha} \sin^2(2\pi\alpha/\lambda_{\alpha})$. When the lattice potential is highly elongated along z -axis (i.e., $V_x = V_y \gg V_z$ and $\lambda_x = \lambda_y \neq \lambda_z$), this 3D atomic gases can be decomposed into an array of independent 1D chains, as seen in Fig. 1. Throughout this paper, we focus on the case when the multiple higher orbitals are partially filled and the lower orbitals are fully occupied, inside each piece well of the optical lattices. Such a high-density filling is attainable, tuning either the total particle number or the confinement of the harmonic trap potential. Amongst the p -orbitals, the Bloch band formed by p_z (i.e., a component along the elongated direction) has a different character from p_x and p_y , as shown in Fig. 1. Hence, we focus on the double degenerate p_x - and p_y -orbitals, hereafter.

Now, we derive a 1D Hamiltonian with p -orbital degeneracy. We first approximate the optical lattice potential, $V_{\text{opt}}(\mathbf{x}) \simeq V_z \sin^2(2\pi z/\lambda_z) + \sum_{\alpha=x,y} V_{\alpha} (2\pi\alpha/\lambda_{\alpha})^2$. Then, we expand the field operator as

$$\psi(\mathbf{x}) = \sum_i \sum_{p=p_x,p_y} c_{p,\sigma,i} u_p(\mathbf{x}_{\perp}) w_i(z), \quad (2)$$

with two kinds of the functions u_p and w_i . The former is the exact solution of $h_{\perp} u_p = \epsilon_p u_p$, with $h_{\perp} = [-(\hbar^2/2m)\nabla_{\perp}^2 + \sum_{\alpha=x,y} V_{\alpha} (2\pi\alpha/\lambda_{\alpha})^2]$, and the latter is the Wannier function formed by the optical lattice potential. Using the tight-binding approximation, we obtain

$$H = \sum_{p,\sigma} \sum_{\langle i,j \rangle} h_{p,\sigma,i,j}^{(t)} + \sum_{p,\sigma,i} h_{p,\sigma,i}^{(\mu)} + \sum_{p,p',i} h_{p,p',i}^{(U)}, \quad (3)$$

with

$$\begin{aligned} h_{p,\sigma,i,j}^{(t)} &= -t c_{p,\sigma,i}^{\dagger} c_{p,\sigma,j}, \\ h_{p,\sigma,i}^{(\mu)} &= -\bar{\mu} n_{p,\sigma,i}, \\ h_{p,p'=p,i}^{(U)} &= U_{pp} \left(n_{p,\uparrow,i} - \frac{1}{2} \right) \left(n_{p,\downarrow,i} - \frac{1}{2} \right), \\ h_{p,p' \neq p,i}^{(U)} &= U_{pp'} \left(\boldsymbol{\rho}_{p,i} \cdot \boldsymbol{\rho}_{p',i} - \mathbf{S}_{p,i} \cdot \mathbf{S}_{p',i} \right), \end{aligned}$$

where $\bar{\mu} = \mu - (U_{pp} + U_{p_x p_y})/2$. The hopping and the on-site interaction energy integrals are defined by, respectively,

$$t = - \int dz w_{i+1} \left(\frac{-\hbar^2}{2M} \frac{d^2}{dz^2} + V_z \sin^2 \frac{2\pi z}{\lambda_z} \right) w_i, \quad (4)$$

$$U_{pp'} = g \int d^3\mathbf{x} w_i^4 u_p^2 u_{p'}^2. \quad (5)$$

The on-site number density of p orbital is $n_{p,\sigma,i} = c_{p,\downarrow,i}^{\dagger} c_{p,\uparrow,i}$. The spin-1/2 operator is $\mathbf{S}_{p,i} = \frac{1}{2} \sum_{\sigma,\sigma'} c_{p,i,\sigma}^{\dagger} \boldsymbol{\tau}_{\sigma,\sigma'} c_{p,i,\sigma'}$, with the 2×2 Pauli matrices $\boldsymbol{\tau} = (\tau^{(x)}, \tau^{(y)}, \tau^{(z)})$, whereas the pseudo spin-1/2 one is defined as

$$\begin{aligned} \rho_{p,j}^{(x)} &= \frac{1}{2} (\rho_{p,j}^{(+)} + \rho_{p,j}^{(-)}), & \rho_{p,j}^{(y)} &= \frac{1}{2i} (\rho_{p,j}^{(+)} - \rho_{p,j}^{(-)}), \\ \rho_{p,j}^{(z)} &= \frac{1}{2} \left(\sum_{\sigma} n_{p,\sigma,j} - 1 \right), \end{aligned}$$

with $\rho_{p,j}^{(+)} = c_{p,\uparrow,j}^{\dagger} c_{p,\downarrow,j}^{\dagger}$ and $\rho_{p,j}^{(-)} = [\rho_{p,j}^{(+)}]^{\dagger}$. Throughout this paper, we use the symbol U_{pp} for representing the intra-orbital interaction strength, since $U_{p_x p_x} = U_{p_y p_y}$. We also find that $U_{p_x p_y} = U_{p_y p_x}$. The intra- and the inter-orbital interaction strength are evaluated by the exact solution of $h_{\perp} u_p = \epsilon_p u_p$. We can find the relation $U_{p_x p_y} = (4/9)U_{pp}$. This relation is also used throughout this paper. In this paper, we set $U_{pp'}$ as a negative value, i.e., an attractive two-body interaction $g < 0$.

The virtue of using the spin representation by $\mathbf{S}_{p,j}$ and $\boldsymbol{\rho}_{p,j}$ in the Hamiltonian is to clarify an underlying symmetry feature of this model. Furthermore, our numerical results are intuitively understood by this representation; in the subsequent sections a fermion-pair particle will be discussed, in terms of $\boldsymbol{\rho}_{p,j}$. Let us here show the symmetry of Eq. (3) explicitly. Taking the summation over p_x and p_y , we build two kinds of operators, $S_i^{(l)} = \sum_p S_{p,i}^{(l)}$ and $\rho_i^{(l)} = \sum_p \rho_{p,i}^{(l)}$, with $l = x, y, z$. We can obtain the operators for $l = \pm$, in a similar manner to the definition of $\boldsymbol{\rho}_{p,j}$. The former is a (local) spin-1 operator, whereas the latter is a (local) pseudo spin-1 operator. After the straightforward calculations, we obtain the algebraic relations,

$$[H, S^{(l)}] = 0, \quad [H, \rho^{(\pm)}] = \mp 2\bar{\mu} \rho^{(\pm)}, \quad [H, \rho^{(z)}] = 0, \quad (6)$$

with $S^{(l)} = \sum_i S_i^{(l)}$ and $\rho^{(l)} = \sum_i \rho_i^{(l)}$. The first one indicates that Hamiltonian (3) is isotropic with respect to

the global spin rotation. The latter two relations mean that this model possesses a highly symmetric property at half filling ($\bar{\mu} = 0$). In other words, the present Hamiltonian has $SU(2)_{\text{spin}} \times SU(2)_{\text{pseudo-spin}} \simeq SO(4)$ symmetry at $\bar{\mu} = 0$.

III. RESULTS

Let us study the quantum phases of Eq. (3) at zero temperature. All the numerical calculations are performed by the DMRG method [13, 14]. Our DMRG code is directly extended toward ladder systems, by parallelizing the superblock matrix diagonalization [30]. The number of states kept is varied from $m = 400$ to maximally 1000 depending on the convergence tendency of the calculations. The boundary condition is open in all the calculations. The subsequent subsection shows the results in a spatially uniform case, without any population imbalance. Next, we turn into the case with spatially uniformity and population imbalance. In the third subsection, the effect of the confinement harmonic trap potential is studied.

A. Zero population imbalance

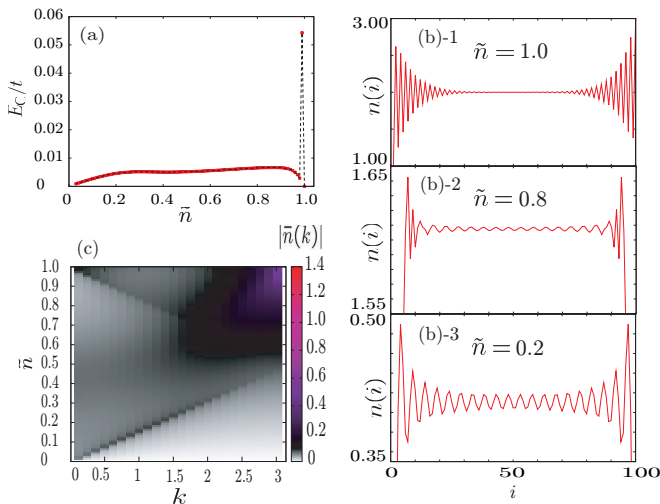


FIG. 2: (Color online) (a) Charge gap E_C versus filling rate \tilde{n} . (b) Particle density $n(i)$, with $\tilde{n} = 1.0, 0.8, 0.2$. (c) Absolute value of the Fourier-transformed density fluctuations, $|\tilde{n}(k)|$ on k - \tilde{n} plane. In all the figures, the population imbalance is $P = 0$, the coupling parameters are $U_{pp} = -10$ and $U_{p_x p_y} = (4/9)U_{pp}$, and the total lattice site number is $L = 100$.

Figure 2(a) shows our DMRG results about the charge gap with respect to the filling rate $\tilde{n} = (1/2L) \sum_i n(i)$, where $n(i) = \sum_{p,\sigma} n_{p,\sigma,i}$ is the particle density and L is the total lattice site number. The charge gap is evaluated by $E_C = E(N + \uparrow\downarrow) + E(N - \uparrow\downarrow) - 2E(N)$, with the

DMRG ground-state energy $E(\cdot)$. In Fig. 2, the population imbalance P is zero; $P \equiv \sum_{p,i} (n_{p,\uparrow,i} - n_{p,\downarrow,i}) = 0$. We find that the charge gap drastically grows up when \tilde{n} is close to half filling (i.e., $\tilde{n} \simeq 1.0$). In contrast, when \tilde{n} decreases from 1, the gap reduces. These behaviors indicate that in this double-degenerate-band attractive 1D model a gapped phase emerges, close to half-filling. We stress that the charge excitation gap does not open in single-band attractive 1D Hubbard chains [16, 17].

We show that the emergence of this charge gap is attributed to the Haldane gap, by mapping the present Hamiltonian onto an interacting spin-1 chain. Using the second order perturbation [29] and the attractive-repulsive transformation [28], we obtain an effective model of Eq. (3), for strong coupling regime $|U_{pp'}| \gg t$. The attractive-repulsive transformation [28] makes Eq. (3) a half-filled system. This transformation is defined by $c_{p,\uparrow,i} = \bar{c}_{p,\uparrow,i}$ and $c_{p,\downarrow,i} = (-1)^i \bar{c}_{p,\downarrow,i}^\dagger$. For the free Hamiltonian $\sum_{p,p',i} h_{p,p',i}^{(U)}$, we obtain

$$H_{\text{eff}} = \sum_{p,\sigma,i} \bar{\mathcal{P}} h_{p,\sigma,i}^{(\mu)} \bar{\mathcal{P}} - \sum_{\substack{p,\sigma,<i,j> \\ p',\sigma',<i',j'>}} V_{p,\sigma,i,j} H_0^{-1} V_{p',\sigma',i',j'}^\dagger, \quad (7)$$

with $V_{p,\sigma,i,j} = \bar{\mathcal{P}} h_{p,\sigma,i,j}^{(t)} \bar{\mathcal{Q}}$. The operators $\bar{\mathcal{P}}$ and $\bar{\mathcal{Q}}$ are, respectively, the projectors onto the subspaces,

$$\bar{\mathcal{H}}_P = \otimes_i \{ |\bar{\uparrow}, \bar{\uparrow}\rangle, |\bar{\downarrow}, \bar{\downarrow}\rangle, (|\bar{\downarrow}, \bar{\uparrow}\rangle + |\bar{\uparrow}, \bar{\downarrow}\rangle) / \sqrt{2} \} \quad (8)$$

$$\bar{\mathcal{H}}_Q = \otimes_i \{ |\bar{\uparrow}, \bar{0}\rangle, |\bar{0}, \bar{\uparrow}\rangle, |\bar{\downarrow}, \bar{0}\rangle, |\bar{0}, \bar{\downarrow}\rangle, |\bar{\uparrow}, \bar{\uparrow}\rangle, |\bar{\uparrow}, \bar{\downarrow}\rangle, |\bar{\downarrow}, \bar{\uparrow}\rangle, |\bar{\downarrow}, \bar{\downarrow}\rangle, |\bar{\uparrow}, \bar{\downarrow}\rangle, |\bar{\downarrow}, \bar{\uparrow}\rangle \}. \quad (9)$$

Here, $|\bar{\cdot}, \bar{\cdot}\rangle$ means $|\bar{\cdot}, \bar{\cdot}\rangle = |\bar{\cdot}\rangle_{p_x} |\bar{\cdot}\rangle_{p_y}$ and the ket vector $|\bar{0}\rangle_{p_x(y)}$ is defined by $\bar{c}_{p_x(y),\sigma,i} |\bar{0}\rangle_{p_x(y)} = 0$. Eq. (7) can be rewritten in terms of the pseudo-spin-1 operators $\rho_i^{(\pm)}$ and $\rho_i^{(z)}$. The effective low-energy Hamiltonian of the system is reduced to a 1D pseudo-spin-1 chain,

$$H_{\text{eff}} = J_{\text{ex}} \sum_{\langle i,j \rangle} \left[\rho_i^{(z)} \rho_j^{(z)} - \frac{1}{2} (\rho_i^{(+)} \rho_j^{(-)} + \rho_i^{(-)} \rho_j^{(+)}) \right] - \sum_i 2\bar{\mu} \rho_i^z, \quad (10)$$

with $J_{\text{ex}} = 2t^2 / (|U_{pp}| + |U_{p_x p_y}|)$. Thus, we find that the charge gap (i.e., the pseudo spin gap) opens, according to Haldane's conjecture [18].

Next, we show another evidence of the Haldane phase in our system. In the open boundary condition, it is well-known that the Haldane phase forms a free half spin state near the boundaries. Figure 2(b)-1 shows that a staggered charge density modulation occurs and exponentially decays toward the bulk region. This behavior corresponds to the $S = 1/2$ edge state [31, 32]. Thus, a free half spin emerges as a free fermion-pair particle, near the edges. This free fermion-pair particle induces a *gapless* charge excitation when the system is the half filling case. Figure 2(a) shows this behavior; the charge

gap occurs right below half filling, whereas a gapless behavior is found at $\tilde{n} = 1.0$. We stress that the gapless behavior at $\tilde{n} = 1.0$ comes from the edge contribution.

Now, we study the case when the filling rate is much lower than half filling. Figures 2(b)-2 and (b)-3 show that the periodic oscillations dominate over the whole spatial region, not only the boundaries, when going below the half filling rate. We obtain the charge density wave (CDW) below half filling. The spatial periodicity indicates the presence of the Luther-Emery phase. If the Luther-Emery phase occurs, the periodicity of the CDW should be characterized by the Fermi wave vector in the equivalent spinless Fermion [33, 34], $2k_F = 2\pi(\rho - |\sum_i \rho_i^{(z)}|/L)$. Here, ρ is pseudo-spin length (i.e., $\rho = 1$). Let us calculate the Fourier transformed density fluctuations, $\bar{n}(k) = \sum_j [n(i) - 2\tilde{n}]e^{ikj}/\sqrt{L}$. Figure 2(c) shows the absolute value $|\bar{n}(k)|$, varying k and \tilde{n} . We find the two kinds of the peaks, a strong peak around $(k, \tilde{n}) \simeq (3.14, 1.0)$ caused by staggered CDW (edge states) and a peak consistent with the prediction of the Luttinger theory $k = 2k_F = 2\pi\tilde{n}$. The latter peak indicates the emergence of the Luther-Emery phase below half-filling. In other words, our model below half filling behaves like an attractive 1D Hubbard chain.

B. Nonzero population imbalance

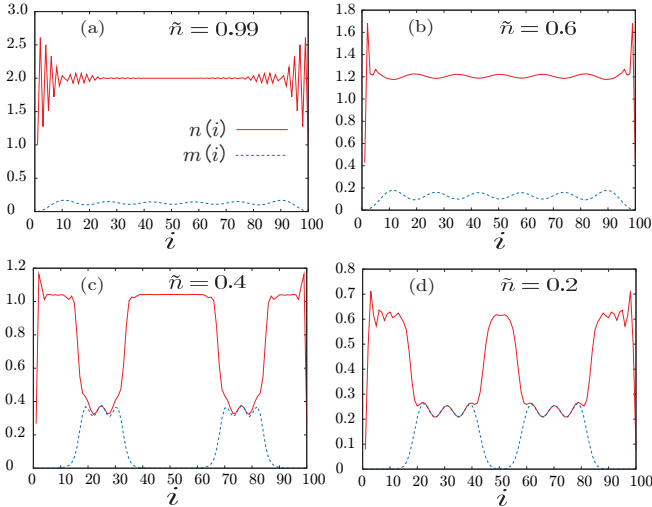


FIG. 3: (Color online) Spatial distributions of the particle density $n(i)$ (solid line) and the spin density $m(i)$ (dashed line), with filling rates (a) $\tilde{n} = 0.99$, (b) $\tilde{n} = 0.6$, (c) $\tilde{n} = 0.4$, and (d) $\tilde{n} = 0.2$. In the all figures, the population imbalance is fixed as $P = 12$. Other physical parameters are the same as in Fig.2.

We study the effects of population imbalance in a spatially uniform case. Figure 3 shows the spatial distributions of the particle density $n(i)$ and the spin density

$m(i) = \sum_p (n_{\uparrow,p,i} - n_{\downarrow,p,i})$, with fixed population imbalance $P = 12$, varying filling rates. At higher filling rates ($\tilde{n} = 0.99, 0.6$), we obtain the spin density wave, as seen in Figs. 3(a,b) (dashed lines). We find that the spatial period is characterized by $2\Delta k_{F,p} = \pi P/L$ (i.e., $2\Delta k_{F,p}L/2\pi = 6$), with the difference of the p -orbital Fermi wave vectors $\Delta k_{F,p} = (\pi/L)\sum_i (n_{p,\uparrow,i} - n_{p,\downarrow,i})$. The density profile depends on the filling rate more sensitively. Right below half filling ($\tilde{n} = 0.99$), a uniform density profile is found in the bulk region, and a staggered CDW occurs at the edges. These results are similar to the case without population imbalance; the charge gap opens in the bulk region, while a free half spin state may induce gapless charge excitations near the boundaries. When the filling rate decreases slightly ($\tilde{n} = 0.6$), a small spatial modulation is found in the whole spatial region. At much lower filling rates ($\tilde{n} = 0.4, 0.2$), we find a drastic effect of the population imbalance. Figures 3(c,d) show a phase separation of polarized components. The small spatial modulation of the particle density for $\tilde{n} = 0.6$ [Fig. 3(b)] is regarded as a precursory phenomenon of this phase separation. Decreasing the filling rate enhances the amplitude of the density-profile oscillation. Then, the low-particle-density regions are created for lower filling rates [35].

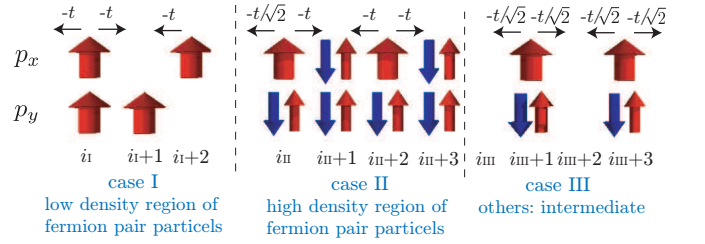


FIG. 4: (Color online) Schematic diagram of hopping processes of unpaired fermions (single up-arrow) in fermion-pair particles (pair of up- and down-arrow).

To clarify the origin of the phase separation, we focus on the kinetics energy of unpaired fermions. Applying the first order perturbation to Eq. (3), we obtain

$$H_K = -t \sum_{p,\sigma} \sum_{\langle i,j \rangle} \mathcal{P}_i \mathcal{P}_j h_{p,\sigma,i,j}^{(t)} \mathcal{P}_i \mathcal{P}_j. \quad (11)$$

The operator \mathcal{P}_i is the projector onto the subspace spanned by the nonzero spin imbalance states and the pseudo-spin-1 states at the spatial site i ,

$$\mathcal{H}_{P>0,\rho=1}^{(i)} = \left\{ |\uparrow, \uparrow\downarrow\rangle, |\uparrow\downarrow, \uparrow\rangle, |\uparrow, 0\rangle, |0, \uparrow\rangle, |\uparrow, \uparrow\rangle, |0, 0\rangle, |\Psi_+\rangle, |\uparrow\downarrow, \uparrow\downarrow\rangle \right\}, \quad (12)$$

with $|\Psi_+\rangle = (|\uparrow\downarrow, 0\rangle + |0, \uparrow\downarrow\rangle)/\sqrt{2}$. The ket vector symbol $|\cdot, \cdot\rangle$ means $|\cdot, \cdot\rangle = |\cdot\rangle_{p_x} |\cdot\rangle_{p_y}$, with $c_{p_x(y),\sigma,i}|0\rangle_{p_x(y)} = 0$. Figure 4 shows hopping processes of the unpaired

Fermion (single up-arrow) embedded in the continuum formed by the fermion-pair particles (pair of up- and down-arrows). If a low fermion-pair-particle-density region spreads, as seen in case I of Fig. 4(b), the transfer probability of the unpaired Fermions is $-t$. This fact is confirmed by, for example,

$${}_{i_{\text{I}+1}}\langle \uparrow, 0 | {}_{i_{\text{I}}}\langle 0, \uparrow | H_{\text{K}} | \uparrow, \uparrow \rangle_{i_{\text{I}}} | 0, 0 \rangle_{i_{\text{I}+1}} = -t.$$

Similarly, in a high fermion-pair-particle-density region [see case II in Fig. 4(b)], the transfer probability is $-t$, since, for example,

$${}_{i_{\text{II}+1}}\langle \uparrow, \uparrow | {}_{i_{\text{II}}}\langle \uparrow, \uparrow | H_{\text{K}} | \uparrow, \uparrow \rangle_{i_{\text{II}}} | \uparrow, \uparrow \rangle_{i_{\text{II}+1}} = -t.$$

In contrast, when the fermion-particle density is intermediate [e.g. CDW-like configuration as case III of Fig. 4(b)], the transfer probability changes, since, for example,

$${}_{i_{\text{III}+1}}\langle \Psi_+ | {}_{i_{\text{III}}}\langle \uparrow, 0 | H_{\text{K}} | 0, 0 \rangle_{i_{\text{III}}} | \uparrow, \uparrow \rangle_{i_{\text{III}+1}} = -t/\sqrt{2}.$$

Thus, the unpaired Fermions prefer to either low or high fermion-pair-particle-density regions.

Now, we apply the above arguments to our numerical results. The second order perturbation terms in Eq. (10) vanish as $J_{\text{ex}} \rightarrow 0$. Furthermore, since the lower filling ($\tilde{n} \ll 1$) means increasing the pseudo magnetic field $2\bar{\mu}$, the pseudo spin-spin interaction of Eq. (10) is irrelevant to the total energy. Thus, the kinetic energy of the unpaired Fermions is predominant, for strong attractive interaction $|U_{pp}| \gg t$ and a lower filling rate ($\tilde{n} \ll 1$). The results shown in Fig. 3 corresponds to the case below half filling (i.e., a low filling case). Therefore, from the consideration about the kinetic energy, the unpaired Fermions in this figure prefer to the low fermion-pair-particle-density regions. In other words, the spin imbalance excludes the fermion-pair particles and leads to a local spin polarized state. This process can be regarded as double exchange interaction [26, 27] between the fermion-pair particles.

C. Harmonic trap potential

We take the effect of the harmonic trap potential into account. The trap potential is typically employed in atomic gas experiments, to avoid the escape of the atoms. When the harmonic trap is considered, we simply add a potential term to our model. Thus, the total Hamiltonian is $H + \sum_{p,\sigma,i} V_{\text{ho}}(i) n_{p,\sigma,i}$, with $V_{\text{ho}}(i) = V[2/(L-1)]^2 [i - (L+1)/2]^2$. We obtain the ground state of this modified Hamiltonian, using the DMRG method.

Figure 5(a1) shows the results, without population imbalance ($P = 0$). The significant feature of the trapped system is the emergence of the Mott core. This result is a contrast to the case of single-band attractive Fermi gases, as seen in Fig. 5(a2); there is no Mott-core structure. This structure implies that the Haldane insulator phase is formed at half filling $n(i) = 2$. From the viewpoint of Eq. (10), the effect of the trap potential is regarded as spatially-dependent pseudo-magnetic field, $\bar{\mu}(i) = \bar{\mu} - V(i)$. Thus, the Mott-core is considered to be a ‘‘magnetization’’ plateau associated with opening of

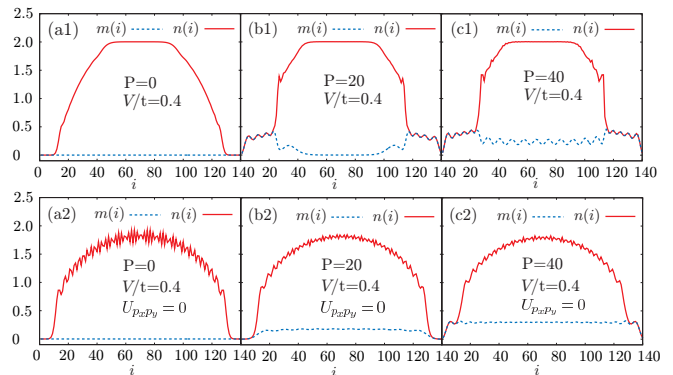


FIG. 5: (Color Online) Spatial distributions of the particle density $n(i)$ (solid line) and the spin density $m(i)$ (dashed line) in harmonic trap potential, with different population imbalances $P = 0, 20, 40$. The trap potential strength is $V/t = 0.4$. The total particle number is 180. The upper panels (a1)–(c1) show the results for the present double degenerate p -orbital 1D chain. For comparison, we show in the lower panels (a2)–(c2) the results for zero intra-orbital interaction ($U_{pxpy} = 0$), i.e., a single-band attractive Hubbard chain.

the Haldane gap. The edge state of the Haldane phase is not observed in our trapped system. The smooth change of this magnetic field leads to the disappearance of the staggered CDW. Below half filling ($n(i) = 2$), the present system is expected to show the CDW oscillation as discussed in section III.A. However, the density oscillation is not sharply observed in Fig. 5.(a1). The 1D single-band case shows a clear CDW oscillation [Fig. 5(a2)]. Therefore, the CDW order in the double degenerate p -orbital system is weaker, compared to the single band case.

Next, we study the results in the presence of population imbalance. Figures 5(b1, c1) show that the Haldane insulator phase occurs, in the same way as the zero population imbalance. Similarly, we find that there is no Mott-core structure, therefore no Haldane insulator phase occurs in a single-band attractive Hubbard chain [Figs. 5(b2,c2)]. The effect of the population imbalance appears, as a phase separation of the polarized components on merge of the trap potential [Fig. 5(b1,c1)]. As discussed in Sec. III B, the kinetic energy of the unpaired Fermions prefers to a low fermion-pair-particle-density region. As a result, the polarized components concentrate at the edges of the trap potential (low density region). The phase separation of the polarized components can be observed in single band attractive Fermi gases with trap potential [36–39] [see Fig. 5(c2), as well]. However, the phase separation in a single-band case is vague, compared to the double degenerate p -orbital system, as seen in Figs. 5(b1,b2). The phase separation of the p -orbital Fermi gases is strong and easily induced by the double exchange interaction between the fermion-pair particles.

Summarizing the results for the trapped system, we can suggest the direct and concrete check of our predic-

tions in experiments. The Mott-core structure is induced by the Haldane gap, and is detectable via the measurement of the particle density profile. The phase separation of the polarized states is identified by comparing the spin density at the trap center to the one at the trap edges. One drawback of the harmonic trap is to erase the edge states related to the Haldane edge states. The realization of box trap potential [40] may capture such states. Observing the string order parameter gives a strong signature of the Haldane insulator phase, as well as measuring the p -band Mott core and the edge states. We suggest that a single-site addressing technique (see, e.g., Ref. [41]) allow a direct check of this quantity. Thus, calculating the string order parameter on the p -band Mott-core is an interesting future work.

IV. SUMMARY

We explored the quantum phases in a 1D p -orbital Fermi gas with attractive interaction, via the DMRG calculations and the mapping onto an effective spin-1 model. To tune the filling rate and the population imbalance in-

duces different phases, including the Haldane insulator phase, the Luther-Emery phase, and the phase separation of the polarized components. We also examined the effect of the harmonic trap potential. We found the emergence of the Mott core structure (i.e., Haldane insulator phase), in spite of attractive Fermi gases. Moreover, the strong phase separation induced by the population imbalance appears at the edges of the trap potential. Thus, the trapped system allows the direct verification of our predictions.

Acknowledgments

We wish to thank Y. Nagai for useful discussions. This research was partially supported by a Grant-in-Aid for Scientific Research from JSPS (Grant No. 23500056). This work was partially supported by the Strategic Programs for Innovative Research, MEXT, and the Computational Materials Science Initiative (CMSI), Japan. We are indebted to T. Toyama for his support. The numerical work was partially performed on Fujitsu BX900 in JAEA. We acknowledge support from the CCSE staff.

-
- [1] I. Bloch, J. Dalibard, and W. Zwerger, *Rev. Mod. Phys.* **80**, 885 (2008); M. Lewenstein, A. Sanpera, B. Damski, A. Sen(De), and U. Sen, *Adv. Phys.* **56**, 243 (2007).
- [2] I. Bloch, J. Dalibard, and S. Nascimbène, *Nature Phys.* **8**, 267 (2012).
- [3] G. Wirth, M. Ölschläger, and A. Hemmerich, *Nature Phys.* **7**, 147 (2011).
- [4] J. Struck, C. C. Ölschläger, R. Le Targat, P. Soltan-Panahi, A. Eckardt, M. Lewenstein, P. Windpassinger, and K. Sengstock, *Science* **333**, 996 (2011).
- [5] T. Müller, S. Fölling, A. Widera, and I. Bloch, *Phys. Rev. Lett.* **99**, 200405 (2007).
- [6] K. Wu and H. Zhai, *Phys. Rev. B* **77**, 174431 (2008).
- [7] C. Wu, *Phys. Rev. Lett.* **100**, 200406 (2008).
- [8] A. V. Gorshkov, M. Hermele, V. Gurarie, C. Xu, P. S. Julienne, J. Ye, P. Zoller, E. Demler, M. D. Lukin, and A. M. Rey, *Nature Phys.* **6**, 289 (2010).
- [9] Zi Cai, Yupeng Wang, and Congjun Wu, *Phys. Rev. A* **83**, 063621 (2011).
- [10] S. Tsuchiya, R. Ganesh, and A. Paramekanti, *Phys. Rev. A* **86**, 033604 (2012).
- [11] K. Kobayashi, M. Okumura, Y. Ota, S. Yamada, and M. Machida, *Phys. Rev. Lett.* **109**, 235302 (2012).
- [12] Xiaopeng Li, Erhai Zhao, and W. Vincent Liu, *Nature Communications*. **4**, 1523 (2013).
- [13] S. R. White, *Phys. Rev. Lett.* **69**, 2863 (1992); *Phys. Rev. B*. **48**, 10345 (1993).
- [14] K. A. Hallberg, *Adv. Phys.* **55**, 477 (2006); U. Schollwöck, *Ann. Phys.* **326**, 96 (2011).
- [15] A. Luther and V. J. Emery, *Phys. Rev. Lett.* **33**, 589 (1974).
- [16] M. Machida, S. Yamada, Y. Ohashi, and H. Matsumoto, *Phys. Rev. A* **74**, 053621 (2006).
- [17] G. Xianlong, M. Rizzi, M. Polini, R. Fazio, M. P. Tosi, V. L. Campo, Jr., and K. Capelle, *Phys. Rev. Lett.* **98**, 030404 (2007).
- [18] F. D. M. Haldane, *Phys. Lett. A* **93**, 464 (1983); *Phys. Rev. Lett.* **50**, 1153 (1983).
- [19] E. G. Dalla Torre, E. Berg, and E. Altman, *Phys. Rev. Lett.* **97**, 260401 (2006).
- [20] E. Berg, E. G. Dalla Torre, T. Giamarchi, and E. Altman, *Phys. Rev. B* **77**, 245119 (2008).
- [21] Y.-W. Lee, *Phys. Rev. B* **77**, 064514 (2008).
- [22] L. Amico, G. Mazzarella, S. Pasini, and F. S. Cataliotti, *New J. Phys.* **12**, 013002 (2010).
- [23] H. Nonne, P. Lecheminant, S. Capponi, G. Roux, and E. Boulat, *Phys. Rev. B* **81**, 020408(R) (2010).
- [24] H. Nonne, P. Lecheminant, S. Capponi, G. Roux, and E. Boulat, *Phys. Rev. B* **84**, 125123 (2011).
- [25] H. Nonne, E. Boulat, S. Capponi, P. Lecheminant, *Phys. Rev. B*. **82**, 155134 (2010).
- [26] L. M. Roth, *Phys. Rev.* **149**, 306, (1966).
- [27] T. Momoi and K. Kubo, *Phys. Rev. B* **58**, R567, (1998).
- [28] R. Micnas, J. Ranninger, and S. Robaszkiewicz, *Rev. Mod. Phys.* **62**, 113 (1990).
- [29] S. Wilson and I. Hubac, *Brillouin-Wigner Methods for Many-Body Systems* (Springer Verlag, 2009).
- [30] S. Yamada, M. Okumura, and M. Machida, *J. Phys. Soc. Jpn.* **78** 094004 (2009).
- [31] I. Affleck, T. Kennedy, E. H. Lieb, and H. Tasaki, *Phys. Rev. Lett.* **59**, 799 (1987); *Commun. Math. Phys.* **115**, 477 (1988).
- [32] S. Miyashita and S. Yamamoto, *Phys. Rev. B* **48**, 913 (1993).
- [33] G. Fath, *Phys. Rev. B* **68**, 134445 (2003).
- [34] T. Giamarchi, *Quantum Physics in One Dimension* (Oxford University Press, New York, 2004).
- [35] Although the phase separation of polarized components

occurs in a uniform system at a low filling rate, the spatial configuration is not fixed. Indeed, we can find that the place of a low-particle-density region depends on the system size L . In the case of a trapped system, the inhomogeneity of the harmonic trap potential determines the spatial configuration of the phase separations.

- [36] A. E. Feiguin and F. Heidrich-Meisner, *Phys. Rev. B* **76**, 220508(R) (2007).
- [37] M. Tezuka and M. Ueda, *Phys. Rev. Lett.* **100**, 110403 (2008).
- [38] G. B. Partridge, W. Li, R. I. Kamar, Y.-A. Liao, and R. G. Hulet, *Science* **311**, 503 (2006).
- [39] Y.-A. Liao, A. Sophie, C. Rittner, T. Paprottam, W. Li, G. B. Partridge, R. G. Hulet, S. K. Baur, and E. J. Mueller, *Nature (London)* **467**, 567 (2010).
- [40] A. L. Gaunt, T. F. Schmidutz, I. Gotlibovych, R. P. Smith, and Z. Hadzibabic, *Phys. Rev. Lett.* **110**, 200406 (2013).
- [41] M. Endres, M. Cheneau, T. Fukuhara, C. Weitenberg, P. Schauß, C. Gross, L. Mazza, M. C. Bañuls, L. Pollet, I. Bloch, and S. Kuhr, *Science* **334**, 200 (2011).